To cite this article: TANG X Y, WAN G B, FU B, et al. A surface for zero-insertion transmission multi-passband frequency selection [J/OL]. Chinese Journal of Ship Research, 2020, 15(5). http://www.ship-research.com/EN/Y2020/V15/I5/79.

DOI: 10.19693/j.issn.1673-3185.01706

A surface for zero-insertion transmission multi-passband frequency selection

TANG Xuying, WAN Guobin, FU Bin, HAN Xianfeng, ZHAO Zhiying*

School of Electronics and Information, Northwestern Polytechnical University, Xi'an 710072, China

Abstract: [**Objectives**] Focusing on the shortcomings of limited band selection and poor control effectiveness of the current multi-band frequency selective surface (FSS), this paper designs a multi-passband frequency selection surface based on the transmission zero insertion method. [**Methods**] The FSS consists of two layers of the same combined structure and a loop patch structure. It has multiple transmission zeros and can control the pass/stopbands independently by adjusting physical parameters. The equivalent circuit model (ECM) is established according to the physical structure of FSS through the ECM method. The full-wave simulation and ECM calculation results can be well fitted. [**Results**] The simulation results show that the designed tri-passband FSS can form passbands in the C, X, and Ku bands. The zero points on both sides of a passband form steep edges and a high-frequency stopband. The stopband enhances out-of-band selection performance. [**Conclusions**] The operating frequency band sees fine polarization stability and angular stability, and the pass/stopbands have a high level of independence.

Key words: frequency selective surface (FSS); multi-passband; transmission zero insertion; equivalent circuit model (ECM); angular stability

CLC number: U665.22

0 Introduction

A frequency selective surface (FSS) is a periodic structure formed by a periodic arrangement of the same elements along one-dimensional or two-dimensional directions. FSSs can select electromagnetic waves of a specific frequency, thus controlling their transmission or reflection. As spatial filters, FSSs have been widely used in controlling electromagnetic compatibility and electromagnetic characteristics of motion platforms such as ships and aircrafts. With the deepening of research, multi-band and multi-passband FSSs have gradually become research hotspots. Multi-band selection can be realized by means of fractal elements, composite elements, and complementary elements. Specifically, fractal elements realize multi-band filtering by forming resonance zones corresponding to different frequency bands through self-similar fractal iteration. Composite elements realize multi-band filtering by arranging conductors of different sizes in a period. Complementary elements realize multi-band filtering through geometric structural complementation and strong interlayer coupling between conductors close to each other.

Core requirements of multi-band FSSs include good and stable filtering characteristics and high controllability of pass/stopbands. However, more pass/stopbands complicate frequency response even more, resulting in worse stability and controllability. Therefore, scholars have put forward various solutions to such a problem. In terms of composite elements, Salehi et al.[1-2] proposed a dual-passband FSS with angular and polarization stability by using square grids and a hybrid resonator. In addition, on the basis of transmission pole-zero control, they further proposed an FSS with a higher-order response and studied technologies for multi-band application of such higher-order FSSs [3]. By optimizing an improved dual square-loop structure, Sivasamy et al. [4]

Received: 2019-08-19 **Accepted:** 2020-03-26

Authors: TANG Xuying, male, born in 1994, master, assistant engineer. Research interests: analysis and design of antenna radomes. E-mail: xuyingtangde@163.com

WAN Guobin, male, born in 1967, professor, doctoral supervisor. Research interests: analysis and design of antenna radomes, antenna theory, and numerical analysis of electromagnetic scattering. E-mail: gbwan@nwpu.edu.cn

***Corresponding author:** WAN Guobin

proposed a dual-band FSS for shielding GSM bands. This structure not only realizes dual-band bandstop but also has excellent angular and polarization stability. Complementary elements have been widely used due to their low profiles and higher-order filtering response. Wang et al. [5] proposed a dual-layer compact FSS based on a square complementary structure, realizing tri-band bandpass filtering. Li et al. [6] proposed a tri-passband FSS combining a convoluted structure with a complementary element, featuring a low profile and a high degree of miniaturization. Based on a cascade connection between a Jerusalem-cross array and a combined aperture structure, through dual-band bandpass filtering formed by strong coupling between the two, Payne et al. [7] designed a miniaturized, super low-profile, and highly-selective dual-passband FSS. Moreover, research has also been carried out in terms of fractal elements and composite elements. Majidzadeh et al. [8] proposed a new combined FSS, which can realize multi-band and ultra-wideband filtering. Song et al. [9] proposed a new tri-passband FSS working in Ku, K, and Ka bands. Palange et al. [10] designed a tri-band bandstop FSS using a fractal structure. Ferreira et al. [11] proposed a dual-band narrow-stopband FSS based on specific combinations of multiple semicircles, with good angular and polarization stability. By arranging two bandstop structures in the same period, Hussein et al. [12] designed a dual-band bandpass FSS working in the Ka band, with high transmissivity and selectivity at the same time. In addition, some scholars have integrated the above ideas. Wang et al. [13] proposed a dual-stopband FSS based on a convoluted structure and a composite element, with incident-angle stability of 0°−60° under TE and TM polarization.

Most of the methods proposed at present only aim for a single demand, applicable to specific scenarios. However, in practical engineering applications, multi-band FSSs often need to work in a large incident-angle range and take into account both polarization modes, and each pass/stopband needs to meet its own performance requirements. Therefore, good controllability is required. In view of the above problems, this paper designed dual/tri-passband FSSs based on transmission zero insertion and equivalent circuit model (ECM) and analyzed them in detail.

1 Pass/stop-band control based on transmission zero insertion

From structural and functional points of view, FSSs are mainly divided into two types: one being of a transmissive structure (aperture) with bandpass characteristics and the other being of a reflective structure (patch) with bandstop characteristics. In the case of resonance, the two types form transmission passbands and stopbands respectively. The so-called transmission zero insertion is explained as follows: resonance frequency and interaction of transmissive and reflective structures in the same element are adjusted by reasonably configuring their physical size and spatial relationship. Thus, transmission zeros can be introduced into a wide passband to segment it into two or more narrow passbands. Specifically, the transmissive structure provides a wide transmission passband and the reflective structure provides zeros, jointly forming multi-band bandpass filtering response.

The simplest element of transmission zero insertion is a cascade of a transmissive structure and a reflective structure. Its ECM is shown in Fig. 1. According to ECM analysis, the transmissive structure can be equivalent to a parallel branch composed of capacitor C_1 and inductor L_1; the reflective structure can be equivalent to a series branch composed of capacitor C_2 and inductor L_2; the thin dielectric layer between the two structures is equivalent to a short transmission line with a thickness of t and impedance of $Z_D = Z_D/\sqrt{\varepsilon_r}$; the semi-infinite free space on both sides of the FSS is equivalent to two semi-infinite transmission lines with an impedance of Z_0. In the figure, Z_T and Z_R are impedance of the parallel and series branches, respectively.

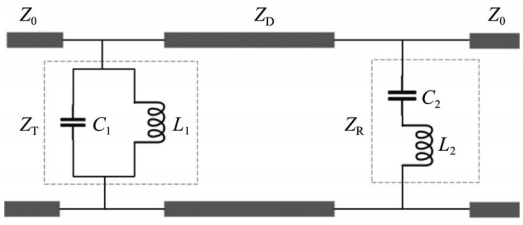

Fig. 1 Equivalent circuit model of the transmission zero insertion structure

Input admittance of the dual-layer cascaded FSS is as follows:

$$Y_{in} = \frac{Z_0 + (1+Z_0)Z_R + j\tan\gamma t(2Z_R+Z_0)}{Z_0Z_TZ_R + jZ_0Z_T(Z_R+Z_0)\tan\gamma t} \quad (1)$$

where Y_{in} is input admittance; Z_0 is the impedance of free space; γ is the equivalent propagation constant of the dielectric layer and for low-loss media, $\gamma = 2\pi\sqrt{\varepsilon_r}/\lambda_0$. Here, ε_r is the dielectric constant of the dielectric layer and λ_0 is the wavelength of an electromagnetic wave in the free space.

As assumed, the transmissive structure has a wide and flat passband, while the reflective structure has a narrow and steep stopband. Due to geometrical complementation between the transmissive and reflective structures, a strong mutual coupling will be formed when the two are connected in parallel. A smaller interlayer spacing leads to stronger mutual coupling. The mutual coupling will influence the resonant frequency of both transmissive and reflective structures, moving resonance-produced passbands and stopbands towards low frequency. Moreover, a stronger coupling field results in a greater influence on the structure. At present, the interlayer coupling of a complementary structure cannot be modeled by equivalent circuits. Therefore, qualitative analysis is carried out to explain the working principle of the transmission-zero-insertion based structure. It is assumed that the transmissive structure in the cascade connection has a passband of $[f_L, f_H]$ centered at f_0, with the highest transmissivity and flatness in a range of $[f'_L, f'_H]$. According to this, the geometric size of the reflective structure is adjusted to make the structure resonant right in this range. In such a case, the stopband of the reflective structure has a central frequency of f_1, with $f_1 \in [f'_L, f'_H]$. In the case of t much less than the wavelength, it can be considered that $\tan\gamma t \approx 0$.

Affected by interlayer coupling, at the frequency f_1, the reflective structure is in a resonant state, while the transmissive structure has not yet formed a complete resonance. In such a case, Z_R=0. As $\tan\gamma t \approx 0$, we have $Y_{in}=\infty$ and input impedance Z_{in}=0. At this time, the whole cascade structure is in a state of total reflection. It is assumed that the transmissivity of the transmissive structure in $[f'_L, f'_H]$ is approximate to 1 and that the transmissive branch has an almost unchanged transmission coefficient, with its Z_T changing at an approximate zero rate. Due to the narrow and steep stopband of the reflective structure, the transmission coefficient changes sharply near f_1, and meanwhile Z_R changes at a high rate. Therefore, when frequency gradually increases or decreases from f_1, Z_R increases rapidly. The corresponding relationship is as follows:

$$Z_T \approx \infty,\ Z_R > 0,\ Z_R \ll Z_T \qquad (2)$$

In such a case, Y_{in} is close to zero and Z_{in} is close to infinity. By analysis, there is a pole on both sides of the transmission zero at f_1; moreover, a narrower stopband of the reflective structure results in sharper changes in Z_R at the edges of the stopband and steeper sidebands of f_1.

When frequency increases or decreases, far away from $[f_L, f_H]$, we have

$$Z_T \approx 0, Z_R \approx \infty \qquad (3)$$

At this time, Z_{in} = 0, and the ECM is in a state of total reflection.

According to the above analysis, the ECM in Fig. 1 has two transmission passbands and one zero between the two passbands, showing dual-band bandpass filtering characteristics, and transition bands on both sides of the zero are narrow. The above conclusions can also be extended to the case of multiple reflective structures with their zeros not close to each other. Therefore, by pass/stopband control based on transmission zero insertion, dual-band or multiband bandpass filtering response can be obtained. In addition, transmission passbands and stopbands can be adjusted by controlling the resonant frequency of transmissive and reflective structures.

2 Design of multi-passband FSSs

2.1 Dual/tri-passband FSSs

Figs. 2-3 show dual-passband and tri-passband FSSs based on transmission zero insertion, respectively. Hexagonal elements with good symmetry and compact arrangement are selected to ensure angular stability of FSSs. The dual-passband FSS consists of three conductor layers and two thin dielectric layers. Specifically, the two FSS1 layers have exactly the same physical size, each consisting of a grid and a loop patch located in the grid. The grid has an inner side of L_1, and the patch has inner and outer sides of L_2 and L_3, respectively. FSS2 has a loop patch with inner and outer sides of L_4 and L_5, respectively. An element has a side length of P. Fillers between conductor layers are media with ε_r of 2.2 and loss tangent of 0.001, which have a thickness of t. An FSS3 of the tri-passband FSS is obtained by loading an additional patch inside the loop patch of an FSS1. In order to ensure angular stability, miniaturized cross-shaped loop patches are selected, with a long edge of L_6, a short edge of L_7, and strip width of w_1. Table 1 lists the physical di-

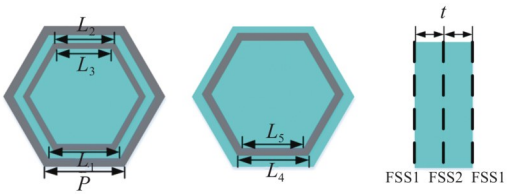

(a) FSS1 (b) FSS2 (c) FSS interlayer structure

Fig. 2 Dual-passband FSS structure diagram

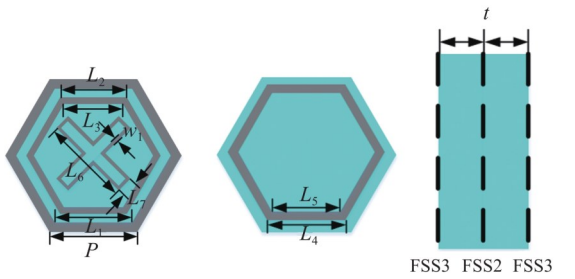

(a) FSS1 (b) FSS2 (c) FSS interlayer structure

Fig. 3 Tri-passband FSS structure diagram

Table 1 Physical parameters of dual/tri-passband FSSs

Physical parameter	Value/mm	Physical parameter	Value/mm
P	5.16	L_5	3.50
L_1	5.04	L_6	4.38
L_2	3.61	L_7	0.97
L_3	3.31	w_1	0.41
L_4	4.19	t	1.20

mensions of the two FSSs.

Fig. 4 shows transmission curves of dual/tri-passband FSSs and dual-passband FSS1-cascaded structure in the case of vertical incidence. In the figure, Zero 1-Zero 4 are four transmission zeros, respectively.

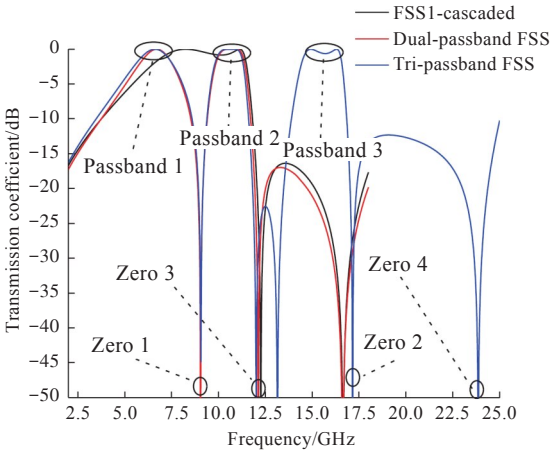

Fig. 4 Transmission curves of dual/tri-passband FSSs and FSS1-cascaded structure

Cascading of the two FSS1 elements forms a wide passband with a range (−1 dB) of 7.07−11.40 GHz and two high-frequency zeros, with a stopband being formed between the zeros. This not only provides a passband wide enough for transmission zero insertion but also improves the out-of-band cutoff performance of the high-frequency end. Resonance of the loop patch of FSS2 produces Zero 1 at 9.05 GHz in the passband, segmenting the wide passband. Passband 1 at low frequency is relatively smooth, and the transition band is wide. Passband 2 at high frequency is between zeros, with steep cut-off zones on both sides, showing good selection performance. Zero 3 at high frequency in Passband 2 is formed by loop patches inside FSS1.

After loading of the cross-shaped loop patch, Passband 3 is formed at high frequency, with a range (−1 dB) of 14.56−16.51 GHz. Individual simulation of the cross-shaped loop patch shows that the resonant frequency of the patch is Zero 2. Similar to Passband 2, Passband 3 is also between zeros. Therefore, Passband 3 has steep sidebands, and a wide stopband is also formed at high frequency. Zero 4 is located on the high-frequency side of Zero 2, jointly formed by the cross-shaped loop patches of FSS3 and the loop patch of FSS2. It together with Zero 2 forms a wide stopband extending to 23.75 GHz, effectively suppressing high-frequency grating lobes. It can be seen that the tri-passband FSS retains high in-band flatness and good selection performance. Moreover, due to the insignificant influence of Passband 3 on frequency and bandwidth of low-frequency passbands, the tri-passband FSS has good inter-band independence and thus a low difficulty of optimization. Its performance parameters are shown in Table 2.

Table 2 Performance parameters of tri-passband FSS

	Passband range(−1 dB)/GHz	Bandwidth/GHz
Passband 1	5.94~7.24	1.30
Passband 2	9.95~11.22	1.27
Passband 3	14.56~16.51	1.95

2.2 Analysis based on ECM

The ECM method is an approximation method that uses lumped circuits for FSS description and equivalent transformation, which can better analyze the filtering characteristics of FSSs. This method has been widely used due to its good applicability. Fig. 5 shows ECMs of the dual/tri-passband FSSs.

An FSS1 in the dual-passband FSS is a hexagon of gridded square-loop structure [14]. According to the equivalent circuit theory, a grid can be equivalent to inductor L_1; the loop patch loaded in the grid can be equivalent to a series branch that is composed of inductor L_2 and capacitor C_1, in parallel with L_1; the patch of FSS2 can be equivalent to a series branch composed of inductor L_M and capacitor C_M; media between conductor layers can be equivalent to short transmission lines with a length of t and impedance of $Z_T = Z_0\sqrt{\varepsilon_r}$. In the tri-passband FSS, a loaded cross-shaped loop patch is equivalent

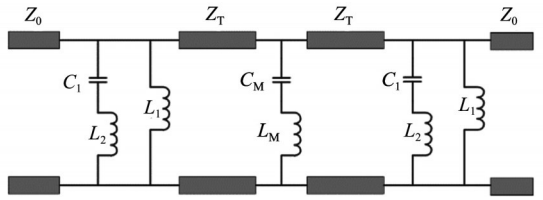

(a) ECM of dual-passband FSS

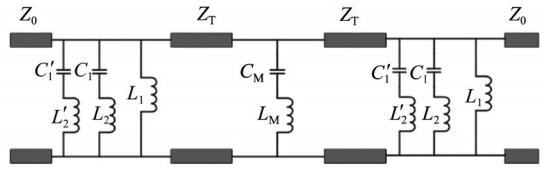

(b) ECM of tri-passband FSS

Fig. 5 ECM of dual/tri-passband FSSs

to a series branch composed of inductor L'_2 and capacitor C'_1.

The formation of Passband 3 can be analyzed in terms of equivalent circuits by referring to Reference [15]. The series branches composed of C_1 and L_2, as well as C'_1 and L'_2, resonate at Zero 1 and Zero 2, respectively. In the case of frequency lower than the resonant frequency, the series branches show capacitive reactance, while in the case of frequency higher than the resonant frequency, they show inductive reactance. Therefore, when the frequency is between Zero 1 and Zero 2, the two branches are in inductive and capacitive states respectively, forming an LC parallel resonator and then Passband 3.

Due to the use of hexagonal elements, parameters of equivalent components cannot be accurately calculated by empirical formulas. Therefore, parameters of reactance components were obtained by particle swarm optimization based on ECMs, as listed in Table 3. In combination with the circuit forms and the parameters of reactance components, ECM transmission curves were calculated through Matlab and then compared with full-wave simulation results, as shown in Fig. 6. As can be seen from the figure, ECM curves of dual/tri-passband FSSs are in good agreement with full-wave simulation results, both having basically the same passbands and stopbands. The difference mainly lies in the number and frequency of zeros, and it is more obvious at high frequency. In the case of a thin dielectric layer, mutual coupling between adjacent conductor layers shifts the working frequency of each structure, while the ECM in Fig. 5 ignores interlayer coupling. This is the main reason for the difference between the ECM curves and the full-wave simulation results. However, the multi-band bandpass filtering in this paper is formed by the independent operation of various structures in elements. Interlayer mutual coupling is only the interference in the case of a thin dielectric layer, and thus it can be ignored in analyzing filtering characteristics. The consistency between the ECM curves and the full-wave simulation results proves the effectiveness of the ECM method.

Table 3 ECM parameters of dual/tri-passband FSSs

Equivalent component	Value
L_1/H	3.79×10^{-9}
L_2/H	4.71×10^{-9}
L'_2/H	3.25×10^{-9}
C_1/F	3.40×10^{-14}
C'_1/F	2.50×10^{-14}
L_M/H	1.00×10^{-8}
C_M/F	3.10×10^{-14}

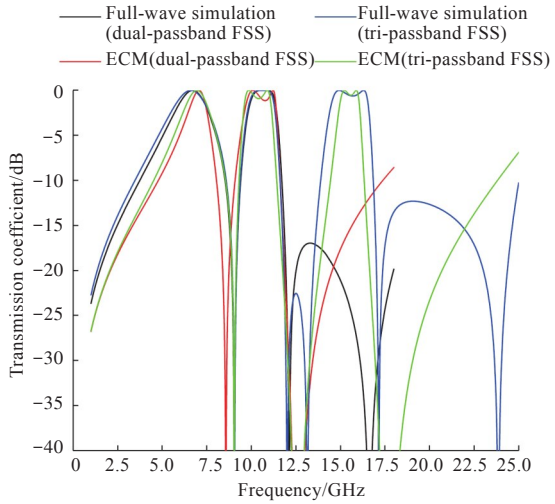

Fig. 6 Transmission curves of dual/tri-passband FSSs from full-wave and ECM simulation

It should be noted that, although it is theoretically feasible to form more high-frequency passbands by loading more reflective structures resonating at high frequency, there is an upper limit on the number of passbands. A high-frequency grating lobe (also known as spurious resonance) formed by Passband 1 is located at high frequency. In the case of oblique incidence, the grating-lobe frequency gradually decreases with the increase in the incident angle. This will seriously worsen the transmission effects of high-frequency passbands formed by reflective structures. Therefore, when FSSs need to work under oblique incidence or in a wide incident-angle range, the number of passbands that can be formed by the method in this paper is limited.

3 Simulation analysis

Fig. 7 shows transmission curves of tri-passband FSSs with changed L_4 and L_6, respectively, in the case of vertical incidence. Fig. 8 shows the transmission curves of tri-passband FSSs in the case of incident angles between 0° and 45°.

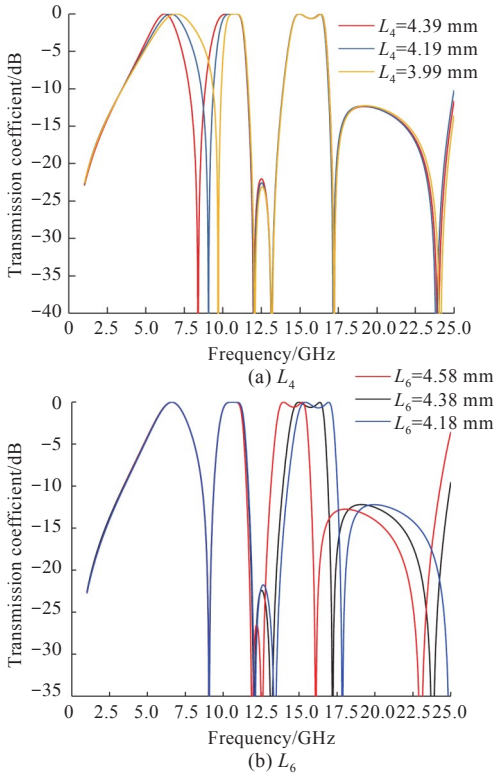

Fig. 7 Variation of tri-passband FSSs transmission coefficients with respect to L_4, and L_6

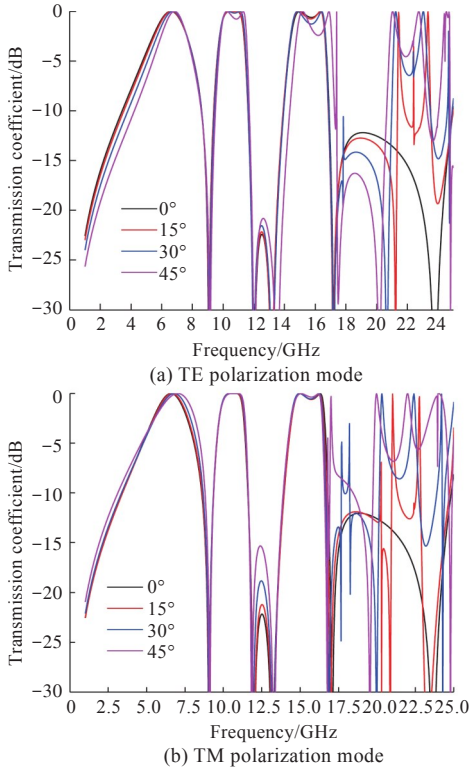

Fig. 8 Variation of transmission coefficients of tri-passband FSSs with respect to the incident angle

The frequency of Zero 1 is controlled by the size of the hexagonal loop in the FSS2. When L_4 decreases, Zero 1 moves to the high-frequency end. As a result, the central frequency of Passband 1 and Passband 2 increases accordingly, with their bandwidth being increased and decreased respectively. The frequency range of Passband 3 is controlled by the size of the cross-shaped loop patch in an FSS3. When L_6 decreases, Zero 2 and Passband 3 move to the high-frequency end at the same time, gradually widening Passband 3. Moreover, when Passband 3 changes with L_6, the insertion loss in the passband remains basically unchanged.

In the case of oblique incidence, transmission curves under different polarization modes have good conformability and wide common passbands. As a high-frequency passband is closer to a high-frequency grating lobe than a low-frequency passband, with the increase in the incident angle, when grating-lobe frequency moves to the low-frequency end, Passband 3 is less stable than Passband 1 and Passband 2. In the case of an incident angle of 45°, all passbands can still maintain common bandwidth under different polarization. This proves good angular and polarization stability of the tri-passband FSS.

4 Conclusion

In this paper, based on transmission zero insertion, dual/tri-passband frequency selection was realized through a combination of bandstop and bandpass structures in the same layer and different layers. In addition, the principle of this method was analyzed based on the ECM method, suitable for an incidence range of 0° −45° and two polarization modes. Specifically, a tri-passband FSS has passbands in the C, X, and Ku bands, as well as multiple zeros between the passbands. The zeros form transmission cutoff effects on both sides of the passbands, effectively shortening transition bands and improving selection performance. Zeros at high frequency form a wide stopband, effectively suppressing a high-frequency grating lobe. Simulation results show that FSSs proposed in this paper have angular and polarization stability in a range of 0°−45° and can independently control pass/stopbands.

References

[1] SALEHI M, BEHDAD N. A second-order dual X-/Ka-band frequency selective surface [J]. IEEE Microwave and Wireless Components Letters, 2008, 18 (12): 785−

787.

[2] GAO M, ABADI S M A M H, BEHDAD N. A dual-band, inductively coupled miniaturized-element frequency selective surface with higher order bandpass response [J]. IEEE Transactions on Antennas and Propagation, 2016, 64 (8): 3729−3734.

[3] LI M, BEHDAD N. Design of low profile single/dual band high-order frequency selective surfaces [C] //Proceedings of 2010 IEEE Antennas and Propagation Society International Symposium. Toronto: IEEE, 2010.

[4] SIVASAMY R, MURUGASAMY L, KANAGASABAI M, et al. A low-profile paper substrate-based dual-band FSS for GSM shielding [J]. IEEE Transactions on Electromagnetic Compatibility, 2016, 58 (2): 611−614.

[5] WANG D S, CHE W Q, CHANG Y M, et al. A lowprofile frequency selective surface with controllable triband characteristics [J]. IEEE Antennas and Wireless Propagation Letters, 2013, 12: 468−471.

[6] LI W X, LI Y Y, GUO X L, et al. A novel miniaturized low-profile tri-band frequency selective surface based on complementary structure [C] //Proceedings of 2016 IEEE International Symposium on Antennas and Propagation (APSURSI). Fajardo: IEEE, 2016.

[7] PAYNE K, CHOI J H, ALI M A, et al. Highly-selective miniaturized first-order low-profile dual-band frequency selective surface [C] //Proceedings of 2016 IEEE International Symposium on Antennas and Propagation. Fajardo: IEEE, 2016.

[8] MAJIDZADEH M, GHOBADI C, NOURINIA J. Novel single layer reconfigurable frequency selective surface with UWB and multi-band modes of operation [J]. AEU-International Journal of Electronics and Communications, 2016, 70 (2): 151−161.

[9] SONG X Y, YAN Z H, ZHANG T L. Triband frequency-selective surface as subreflector in Ku-, K-, and Ka-bands [J]. IEEE Antennas and Wireless Propagation Letters, 2016, 15: 1869−1872.

[10] PALANGE A K, SONKER A, YADAV S S. Designing of multiband frequency selective surfaces [C] //Proceedings of 2016 International Conference on Communication and Signal Processing. Melmaruvathur: IEEE, 2016: 491−494.

[11] FERREIRA D, CUINAS I, FERNANDES T R. et al Multi-semicircle-based single-and dual-band frequencyselective surfaces: achieving narrower bandwidth and improved oblique incidence angular stability [J]. IEEE Antennas and Propagation Magazine, 2019, 61 (2): 32−39.

[12] HUSSEIN M, HUANG Y, AL-JUBOORI B, et al. A multi-band high selectivity frequency selective surface for ka-band applications [C] //Proceedings of 2017 10th Global Symposium on Millimeter-waves. Hong Kong, China: IEEE, 2017.

[13] WANG N N, DU T Y, ZHAO B X, et al. A closely located dual-band FSS with frequency stability for multi-frequency communication [C] //Proceedings of International Symposium on Antennas and Propagation (ISAP). Phuket: IEEE, 2017.

[14] LIU S S, GAO Z P. Equivalent circuit model of multilayer square frequency selective surface absorbing material [J]. Materials Review, 2015, 29 (22): 130−134, 140 (in Chinese).

[15] YAN M, WANG J, MA H, et al. A tri-band, highly selective, bandpass FSS using cascaded multilayer loop arrays [J]. IEEE Transactions on Antennas & Propagation, 2016, 64 (5): 2046−2049.

一种基于传输零点插入的多通带频率选择表面

唐旭英，万国宾*，付斌，韩先锋，赵志颖

西北工业大学 电子信息学院，陕西 西安 710072

摘　要：［**目的**］针对目前多频段频率选择表面存在的通/阻带选择性能有限、调控效果差的缺点，基于传输零点插入方法，设计一种多通带频率选择表面（FSS）。［**方法**］FSS 单元由 2 层相同的组合结构和 1 层环形贴片结构组成，具有多个传输零点，可以通过调整物理尺寸实现对通/阻带频率的独立控制。基于 FSS 的等效电路法，按照其物理结构建立等效电路模型并进行分析，全波仿真与等效电路法（ECM）计算结果可以很好地拟合。［**结果**］仿真结果表明，所设计的三通带 FSS 可在 C，X，Ku 频段内形成 3 个传输通带，位于通带两侧的零点形成了陡峭的边沿，缩短了过渡带，高频零点形成了宽传输阻带，进一步提升了带外选择性能。［**结论**］所设计的 FSS 在工作频段内具有良好的极化稳定性和角度稳定性，且通/阻带独立性较好。

关键词：频率选择表面；多通带；传输零点插入；等效电路模型；角度稳定性